Exploration of Occurrence and Energetics of EPBs

Alanah Cardenas-O'Toole, Shasha Zou, Mary Smirnova, and Grace Kwon

University of Michigan Department of Climate and Space Sciences and Engineering

CEDAR 2026

EQIT-5

alanahco@umich.edu

1. Background and Motivation

Equatorial Plasma Bubbles (EPBs) are density depletions in the F-region ionosphere (Woodman & La Hoz, 1976) starting as perturbations at the magnetic equator and expanding along magnetic flux tubes (Tsunoda, 1980) that are commonly attributed to the Rayleigh-Taylor (R-T) Instability (Tsunoda, 1985). As they grow in altitude and latitude, they may bifurcate into small-scale irregularities (e.g., Yokoyama et al., 2014), causing disruptions to satellite navigation and communication (Aarons, 1982). Observationally, they have been detected up to ~45°N magnetic latitude (MLat) (e.g., Aa et al., 2018) and may be a source of mid and low latitude scintillation (Sousasantos et al., 2023). **This underscores the importance of the continued study of this phenomenon from a space weather forecasting, agricultural, and military perspective.**

In this analysis, we discuss our EPB detection algorithm using 1 Hz in situ Swarm plasma density (N_p) data and analyze the properties and electron temperature (T_e) of EPBs during solar maximum from January 2022 through December 2025. While many studies explore EPBs and their properties, the bubble temperature is underrepresented in literature due to the difficulty of measuring plasma temperature reliably. **Understanding the temperature and the occurrence of EPBs, particularly those extending into midlatitudes, allows the community to corroborate model studies, find characteristics unique to EPBs, and eventually understand the life-cycle of EPBs.**

2. Detection Algorithm

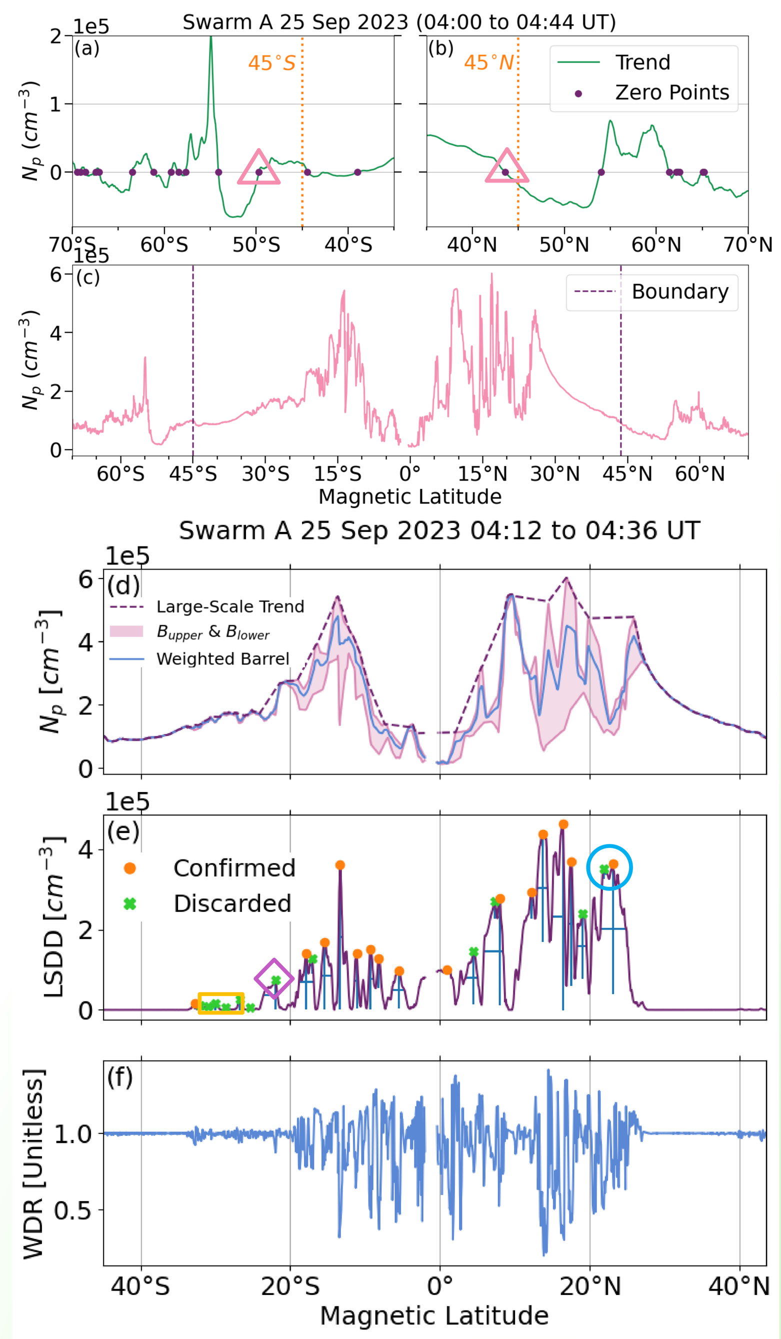

Figure 1: Swarm A N_p detrending method

i) Limit Search

EPB search is limited to ±45° MLat unless the equatorward boundary of the midlatitude trough is found at a lower MLat. We adapted the method from Liu and Xiong (2020) by searching N_p from ± 70° to ±35° MLat (Fig 1a and 1b) and applying large- (320s) and small-scale (10s) moving averages and subtracting them. Zero points (purple dots) are paired around minima. If one or both zero points have a 40% depth, they are set as trough edges (pink triangles show equatorward boundary).

ii) Detrend Density

To detrend N_p, we adapted a barrel roll method (Fig 1c), which was developed by Pradipta et al. (2015) and expanded by Wan et al. (2024).

Large-Scale Trend

- Apply five barrels with decreasing radii (80s to 16s) rolling bi-directionally atop N_p (Fig 1d).
- Subtract N_p from the large-scale trend to get the Large-Scale Density Difference (LSDD) and apply a 5s mean filter (Fig1e).
- Look for peaks using Python's find_peaks with a minimum $5x10^3$ cm^{-3} prominence and 40 km width.
- **The peaks are Equatorial Plasma Irregularity (EPI) candidates.**

Small-Scale Trend

- Apply five barrels with increasing radii (8s to 40s) rolling bi-directionally atop (B_{upper}) and under (B_{lower}) N_p (Fig 1d).
- Create weighted barrel (*WB*)

$$WB = \frac{2 \times B_{upper} + B_{lower}}{3}$$

- B_{upper} is weighted more heavily because it emphasizes depletions over increases.
- B_{lower} is included because a sudden increase in density may result in artificial depletion in B_{upper}.
- Dividing the N_p by weighted barrel creates the Weighted Density Ratio (WDR) (Fig 1f).
- **The WDR indicates the presence or absence of irregularities.**

iii) Test Candidates

Test EPI candidates to ensure most detections are not artificial or non-bubble irregularities.

- The **depth check** (Fig 1e yellow box) removes small non-bubble irregularities using the LSDD maximum and percent depth ($\%_{depth}$).
- The **nested bubble check** (Fig 1e blue circle) removes small and shallow irregularities inside larger ones.
- The **WDR check** (Fig 1e purple diamond) removes artificial irregularities created by detrending that often occur with a sudden increase in N_p.
- The **frequency check** (Fig 2) removes artificial irregularities due to potentially problematic data by applying a sliding Fourier transform to 20s ΔN_p and removing points with a maximum frequency over 0.2 Hz.

$$\%_{depth} = \frac{LSDD - N_p}{LSDD} \times 100\%$$

$$20s\ \Delta N_p = \frac{N_p - 20s\ Filtered\ N_p}{N_p}$$

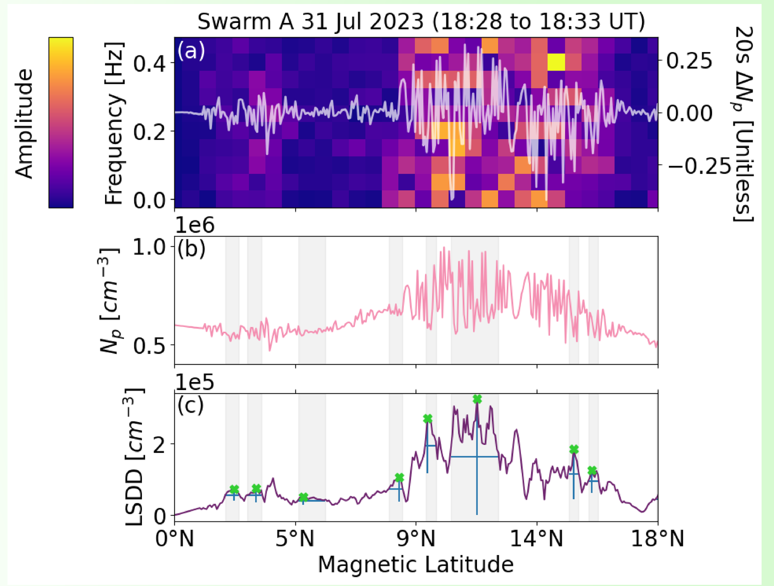

Figure 2: Fourier Transform applied to problematic data

iv) Confirm EPI

If a detection meets all criteria, it is considered an equatorial plasma irregularity (EPI) as outlined in the flowchart below. EPI and candidate information on the width, prominence, magnetic and geographic coordinates, $\%_{depth}$, WDR, and bubble center T_e and edge T_e are some of the characteristics saved in the EPI database. Flags are added for suspicious detections including depletions found $> \pm 25°\ MLat$ with no low latitude counterparts. For the statistical analysis, EPIs between ±40° MLat were selected to ensure sufficient data points entering the analysis. EPIs at higher MLats need to be examined carefully on a case-by-case basis.

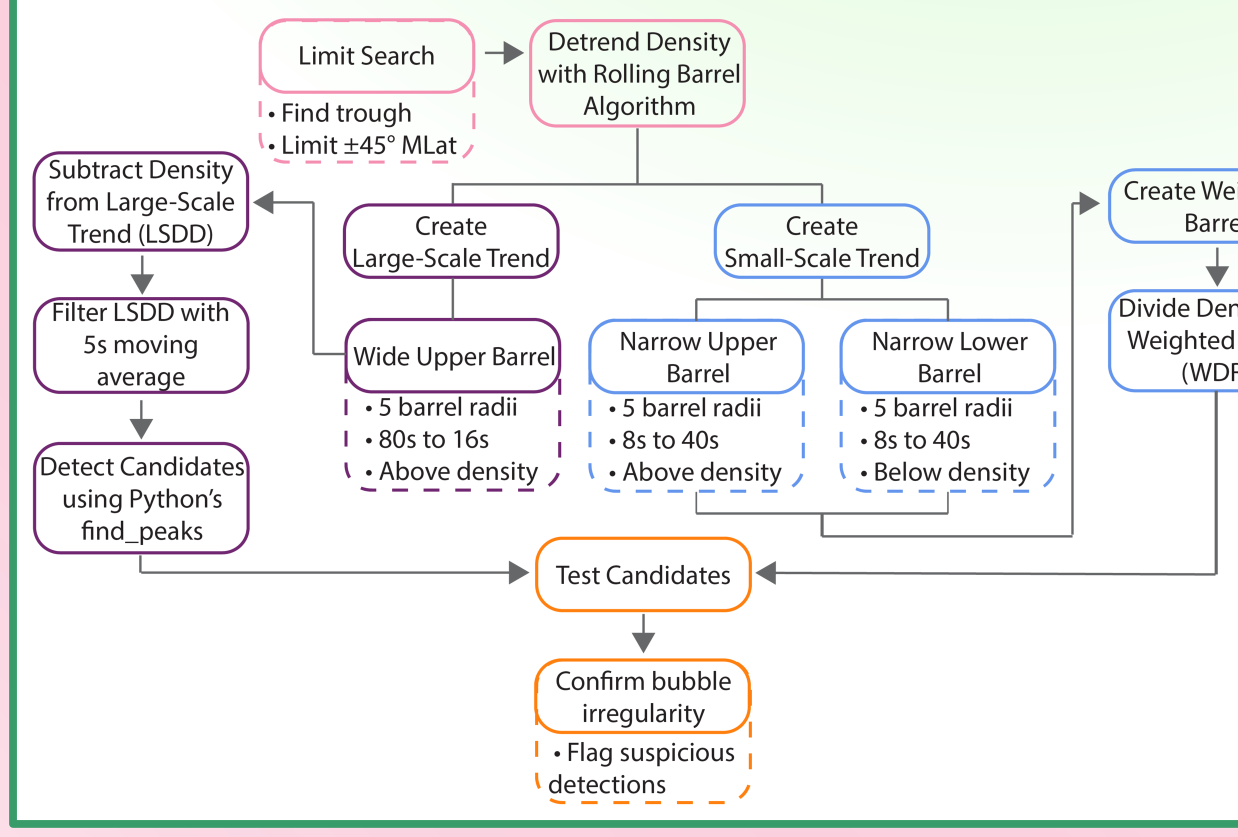

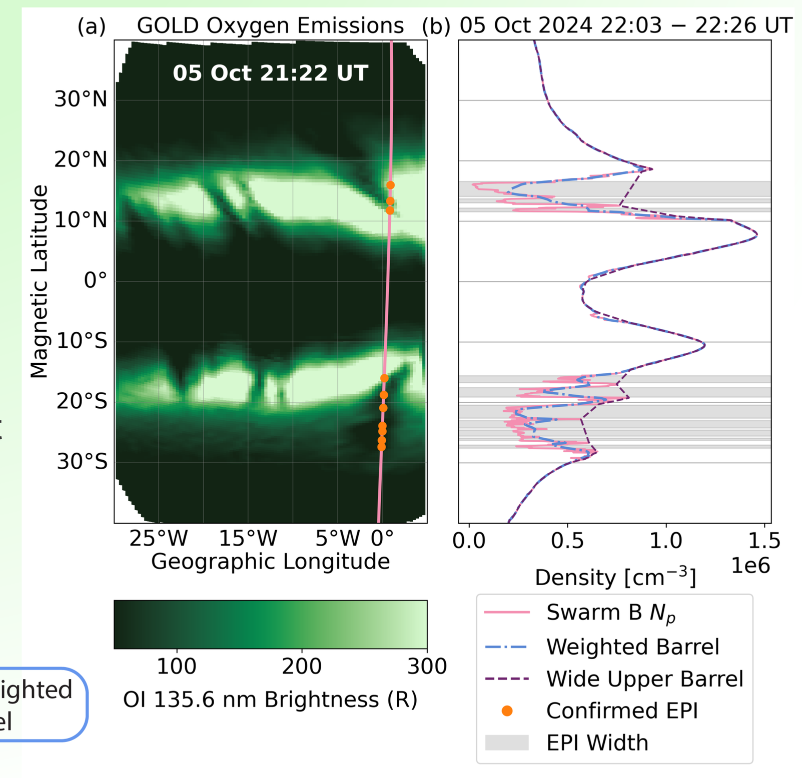

Figure 3: Swarm EPI detection paired with GOLD Oxygen Emissions

Fig 3 shows an example of GOLD oxygen emissions on 05 October 2024 at 21:22 UT. Swarm B passed the same longitude from 22:03 to 22:26 UT. The detection algorithm, detected 10 EPIs that match the GOLD observations. All EPI detections appear to be from the same bubble, which is why it is important to differentiate that these are bubble irregularities (EPIs) and not individual bubbles (EPBs).

3. Occurrence and Energetics

- From 01 January 2022 to 31 December 2025, Swarm C detected 29,434 EPIs between ±40° MLat from 18 to 11 Local Time (LT).
  - **(Fig 4c) There is a quick decrease in prominence (LSDD maximum) before 22 LT, possibly from the F-region density decay due to chemical recombination.**
  - As the F-region becomes more depleted, recombination slows as the rate is proportional to the density shown from 22 to 02 LT (Fig 4c).
  - (Fig 4d) A line was fit to the normalized prominence and depth (Fig 4b) for each LT.
    - Before 22 LT, the comparatively large slopes (> 0.2) may result from the relationship between the recombination in the background and in the bubble.
    - As the night progresses to 04 LT, the background N_p reaches its diurnal minimum, and the bubble prominence decreases because the ambient plasma has depleted.
    - **After 05 LT, the F-region starts to repopulate from renewed photoionization, thus a higher correlation between the background and bubble N_p emerges.**
- About ¼ of the EPI detections from Swarm contained reliable T_e measurements determined by removing flagged data, outliers, and 30s after each instrument sweep, which caused an artificial increase.
  - (Fig 5a) **A distinct increase in T_e (05 – 06 LT)** and decrease in T_e (~ 08 LT) occurs as the morning overshoot also observed in the background plasma (Oyama et al., 1996).
  - (Fig 5b) **The heating due to solar irradiance absorption starts earlier in solstice months likely due to the predawn effect** (e.g., Oyama et al., 1996), where photoelectrons travel along field lines from the dark to sunlit hemisphere causing heating in dark hemisphere at earlier LTs.
  - (Fig 5c – g) Heating starts earlier during solstice months but is quicker in equinox months likely due to the predawn effect.

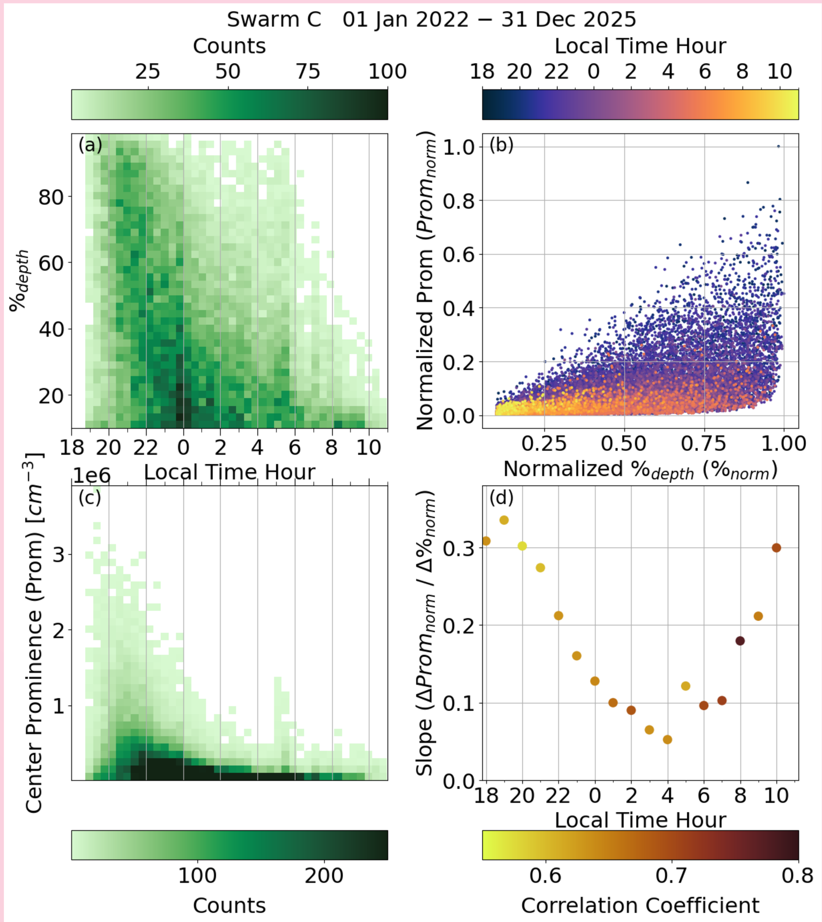

Figure 4: Swarm C EPI (a) $\%_{depth}$ vs LT, (b) Normalized Prom vs Normalized $\%_{depth}$, (c) Prominence vs LT (d) slope and correlation between $Prom_{norm}$ and $\%_{norm}$ per LT.

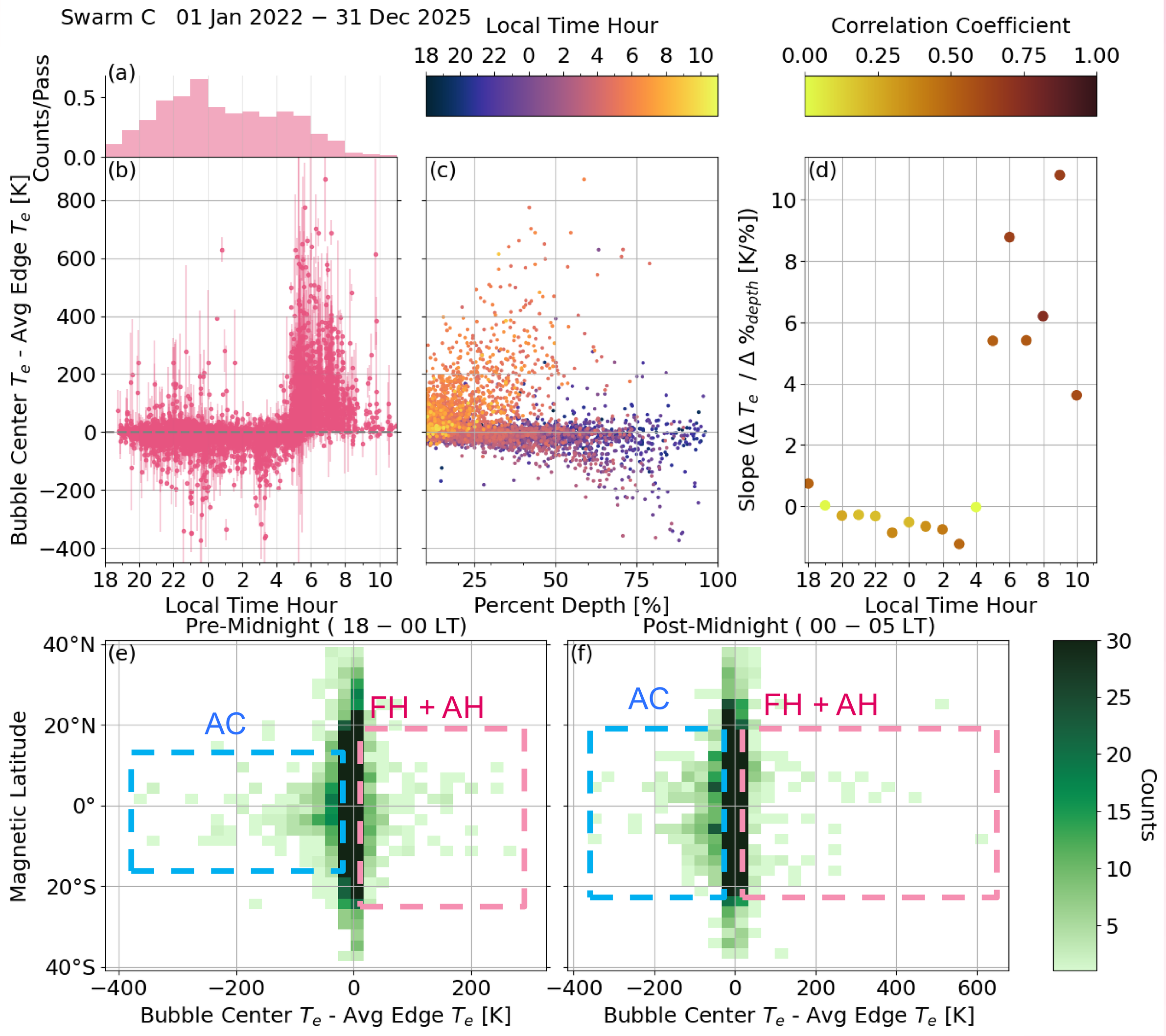

Figure 6: Swarm C EPI (a) LT distribution, (b) ΔT_e versus LT with edge T_e difference divided by two as error bars, (c) ΔT_e vs. $\%_{depth}$, (d) slope between ΔT_e and $\%_{depth}$ vs LT, (e) – (f) ΔT_e by MLat

- During bubble formation, main heating and cooling processes at Swarm altitudes include (Huba et al., 2009):
  - **Adiabatic cooling from flux tube expansion** (Fig 6e, 6f blue "AC").
  - **Adiabatic heating from super fountain effect** (Fig 6e, 6f pink "AH").
  - **Frictional heating from ion-electron collisions** (Fig 6e, 6f pink "FH").

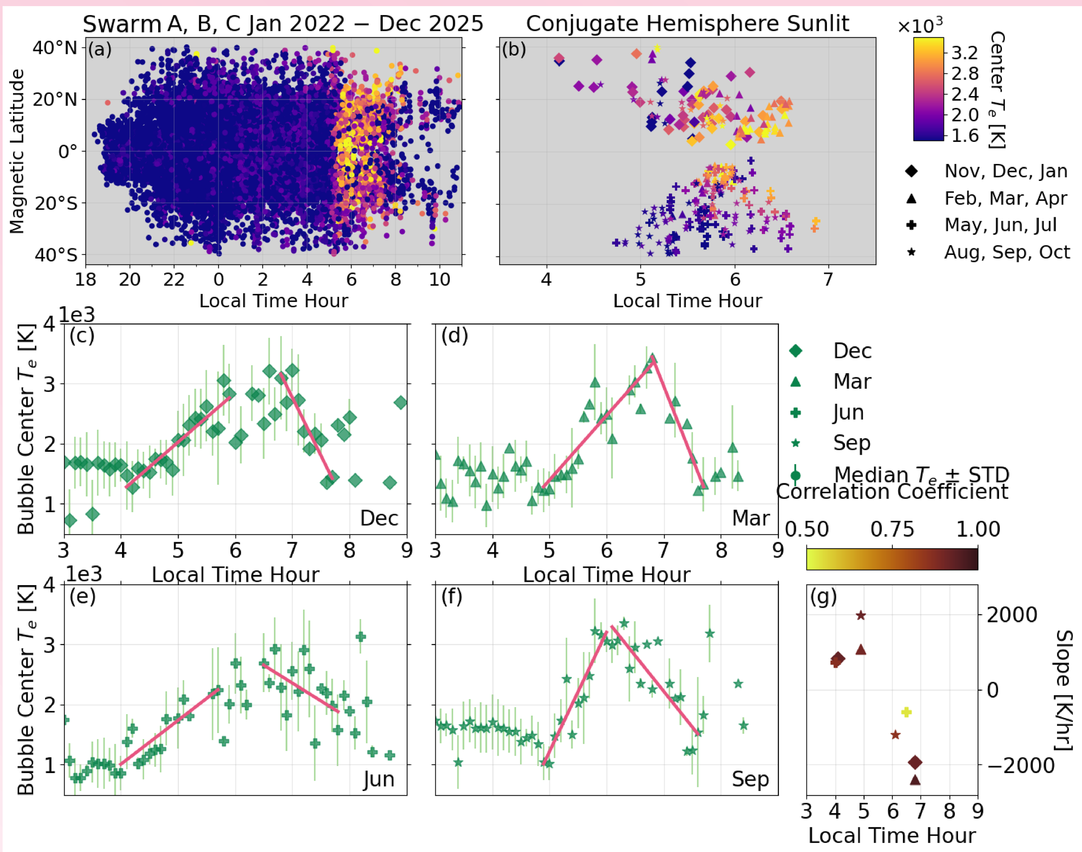

Figure 5: Swarm A, B, and C (a) EPI T_e by LT and MLat. (b) T_e when conjugate hemisphere is sunlit and detection is dark. (c) – (f) Median T_e per 6 LT minutes with linear fits (pink) (g) Slopes of the fits in (c) – (f) by LT.

- (Fig 6a) Sharp increase in bubble center T_e – average edge T_e (ΔT_e) at ~ 05 LT with a maximum ~ 06 LT.
- Also observed by Oyama et al., (1988), who noted that it is likely a result of **photoelectron heating**.
- (Fig 6c and 6d) **ΔT_e is more strongly related to $\%_{depth}$ for dawn and morning LTs.**
- As the ionosphere begins to repopulate, the total incoming solar photon energy has slow variation as solar zenith angle changes, so the heating per electron decreases as N_e increases.

4. Conclusions and Future Work

- **This study provides new insights into the physical and energetic processes associated with bubble dynamics. Our findings map the nocturnal evolution of EPIs, shedding light on the complex, lesser-studied relationship between bubble density depletion and electron temperature variations.**
- We developed a robust EPB detection algorithm.
  - Tracks the prominence, depth, coordinates, width, and temperature for EPIs detected by Swarm A, B, and C.
  - Detected 29,434 EPIs in Swarm C 1 Hz in situ density from 2022 through 2025.
- **We present the most extensive study to date on the relationship between bubble temperature and density.**
  - The LT dependence of the relationship between the ambient and bubble density likely results from recombination (18 – 22 LT) and photoionization (08 – 11 LT) (Fig 4).
  - Bubble heating varies by season with heating occurring sooner during solstices but quicker during equinoxes (Fig 5).
  - ΔT_e varies by LT remaining close to 0 K before 05 LT when sunrise begins and the bubble temperature increases rapidly, which is consistent with photoelectron heating causing the morning overshoot (Fig 5).
  - The depth and temperature difference are more positively related during dawn and morning LTs (Fig 6).
  - There is evidence of adiabatic heating and cooling and frictional heating pre- and post-midnight as modeled by Huba et al. (2009) (Fig 6).
- **In the future, we will analyze the relationship between EPI occurrence and energetics to solar cycle by applying our algorithm to more Swarm data from 2014 through 2025, and we will explore the differences in properties between super and regular EPBs.**
- Additionally, we will work on publishing the detection algorithm to be applied to more datasets.

5. References and Acknowledgements

Aa et al., (2018). Midlatitude plasma bubbles over China and adjacent areas during a magnetic storm on 8 September 2017. doi: https://doi.org/10.1002/2017SW001776

Aarons, J. (1982). Global morphology of ionospheric scintillations. doi: https://doi.org/10.1109/PROC.1982.12314

Huba et al., (2009). Ion and electron temperature evolution during equatorial spread f. doi: https://doi.org/10.1029/2009GL038872

Liu, Y., & Xiong, C. (2020). Morphology evolution of the midlatitude ionospheric trough in nighttime under geomagnetic quiet conditions. doi: https://doi.org/10.1029/2019JA027361

Oyama et al., (1996). Morning overshoot of T_e enhanced by downward plasma drift in the equatorial topside ionosphere. doi: https://doi.org/10.5636/jgg.48.959

Oyama et al, (1988). Temperature structure of plasma bubbles in the low latitude ionosphere around 600 km altitude. doi: https://doi.org/10.1016/0032-0633(88)90025-6

Pradipta et al., (2015). An effective tec data detrending method for the study of equatorial plasma bubbles and traveling ionospheric disturbances. doi: https://doi.org/10.1002/2015JA021723

Sousasantos et al., (2023). Severe l-band scintillation over low-to-mid latitudes caused by an extreme equatorial plasma bubble: joint observations from ground-based monitors and gold. doi: https://doi.org/10.1186/s40623-023-01797-5

Tsunoda, R. T. (1980). Magnetic-field-aligned characteristics of plasma bubbles in the nighttime equatorial ionosphere. doi: https://doi.org/10.1016/00219169(80)90057-4

Tsunoda, R. T. (1985). Control of the seasonal and longitudinal occurrence of equatorial scintillations by the longitudinal gradient in integrated e region Pedersen conductivity. doi: https://doi.org/10.1029/JA090iA01p0044

Wan et al., (2024). An automatic method for detection and naive classification of the martian ionospheric irregularities. https://doi.org/10.1029/2023JA03222

Woodman, R. F., & La Hoz, C. (1976). Radar observations of f region equatorial irregularities. doi: https://doi.org/10.1029/JA081i031p05447

Yokoyama et al., (2014). Nonlinear growth, bifurcation, and pinching of equatorial plasma bubble simulated by three-dimensional high-resolution bubble model. doi: https://doi.org/10.1002/2014JA020708

AC was supported by NASA FINESST 80NSSC22K1847. AC would also like to thank Angeline Burrell, Dustin Hickey, Jeff Klenzing, Mariah Cardenas, and Christopher Thomas for their helpful discussions and suggestions. The Swarm data products are provided by ESA. The GOLD data was provided by NASA.